GEOPHYSICAL RESEARCH LETTERS, VOL. 21, NO. 1, PAGES 29-32, JANUARY 1, 1994

Intergranular basaltic melt is distributed in thin, elogated inclusions

Ulrich H. Faul, Douglas R. Toomey and Harve S. Waff

Department of Geological Sciences, University of Oregon, Eugene

Abstract. We describe a method to analyze the melt distribution in experimentally produced ultramafic partial melts. It is shown that the melt inclusions can be approximated by ellipses in two dimensions and by penny-shaped ellipsoids in three dimensions. The aspect ratios of these ellipses (the ratio of the minor to the major axis) can in turn be used to calculate bulk physical properties of partial melts. We apply this method to two olivine-basalt samples with 3.2% and 0.75% melt fraction. In the samples analyzed approximately 75% of the melt is contained in inclusions with much smaller aspect ratios than triple junction tubules. The reduction of P-wave velocities calculated for this melt distribution is twice as large as for melt distributed solely in triple junction tubules.

Introduction

Knowledge of the melt distribution in partially molten regions of the upper mantle is important for the interpretation of geophysical data and for models of the chemical and dynamic evolution of the upper mantle. When upwelling mantle first crosses the solidus, melt is distributed intergranularly; only after a sufficiently permeable network is established can melt segregate from the solid matrix. Waff and coworkers established that surface tensions between crystalline grains and the melt determine the melt distribution [Bulau et al., 1979, Waff and Bulau 1982]. With the assumption of crystalline isotropy the equilibrium texture is characterized by constant solid-liquid interfacial curvature and a unique wetting or contact angle between solid and liquid. If this wetting angle, θ, has a value between $0° < \theta < 60°$ liquids form an interconnected network of tubules along all three grain edge intersections.

While the wetting angle for olivine-basalt partial melts falls in this range, the observed melt distribution in experimentally produced partial melts differs substantially from the predicted tubule geometry [Waff and Faul, 1992]. Triple junction tubules are present, but much of the melt is located in larger, often thin and elongated melt inclusions. These inclusions are commonly bound by more than three grains and extend deep between grain boundaries. The two main reasons for the latter geometries are the crystalline anisotropy of olivine and pyroxene, the major upper mantle constituent minerals, and the space filling requirements of a polycrystalline aggregate with a range of grain sizes. A more detailed explanation for the experimentally observed textures is given in Waff and Faul [1992]. While for the isotropic model the wetting angle and melt fraction are sufficient to calculate the melt distribution [von Bargen and Waff, 1986], no model exists to predict the distribution of fluids in an anisotropic polycrystalline aggregate. In the absence of such a model this paper presents a method to quantify the observed melt distribution by analyzing backscattered electron (BSE) images of experimentally produced samples. These results can then be used to calculate bulk physical properties of partial melts.

Paper number 93GL03051
0094-8534/94/93GL-03051$03.00

Experimental Conditions, Image Acquisition and Processing

The experiments were conducted in a conventional solid medium piston cylinder apparatus. To preserve the melt distribution at run conditions, the furnace power was turned off with the charge at target pressure and temperature, causing the melt to quench to glass. Charges run with graphite as sample chamber material are often extensively fractured during quench, while sample containers made of iron incurred little or no fracturing. Fractured samples are not suited for the image processing discussed below. For this reason experiments run with high purity iron sample containers were analyzed, despite the diffusion of iron into the sample over the run duration. The post-run iron content of olivine and melt from the two experiments reported here is substantially different, yet their melt distribution is nearly indistinguishable (see below), suggesting that the iron content does not significantly alter the topological distribution of melt. For a detailed description of experimental techniques, furnace assemblies and post run sample preparation see Waff and Bulau [1982]. Experimental conditions are given in Table 1. The sample material of run BL82 is a crushed lherzolite, where sieving removed all pyroxene; only olivine and spinel are found in the polished sample. The starting material for HD87 was 98.5 wt% Hawaiian Dunite mixed with 1.5 wt% alkaline basalt.

The BSE images were obtained from vertical sections through the center of post-run samples with 10 KeV acceleration voltage and 20 nA specimen current. Each image consists of 512 by 512 pixels with a step size of 0.3 μm and 8 bytes per pixel. A total of 36 images were acquired, 16 from BL82 and 20 from HD87. The gray scale images were converted to binary maps with only the melt remaining by a threshold operation or, if necessary, by digitizing the melt on screen. Figure 1 shows an example of a binary image from BL82.

To quantify the distribution of the melt three independent measurements for each inclusion were obtained from the binary images: the area (the sum over all contiguous pixels, A), the perimeter (the length of feature's boundary, P) and the length (defined as the longest chord connecting any two points on the perimeter, L). These fundamental measurements are then used to calculate various derived parameters that characterize the shape of the melt inclusions.

TABLE 1. Experimental Conditions and Material

Run	P, GPa	T, ° C	Duration, hours	Number of inclusions	Melt fraction, %[a]
BL82	1.0	1395	96	306	3.2±0.2
HD87	0.85	1350	216	165	0.75±0.05

[a] Averaged melt fraction from all images of a run

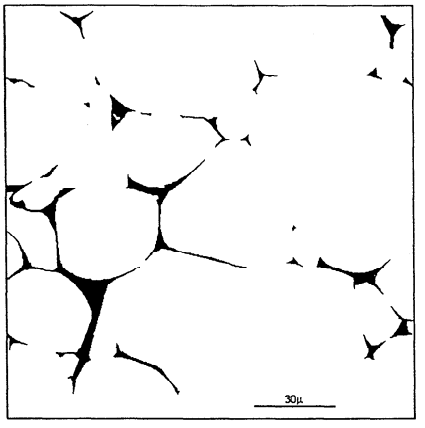

Fig. 1. Example of binary image obtained from run BL82. Black areas represent quenched melt. The fundamental measurements of area, perimeter and length for each separate inclusion are obtained from similar images. Characteristic triple junctions can be seen at the top, but most of the glass resides in larger pockets and low aspect ratio inclusions.

Calculation of the Aspect Ratio of Melt Inclusions

A common measure of the shape of voids or inclusions in crustal rocks is their aspect ratio α, defined as the ratio of the minor axis over the major axis of an ellipse. The aspect ratio is used to describe the shape of voids varying widely in nature, from cracks in granite and gneiss with α as low as 10^{-4} [e.g. Hadley, 1976] to pores in sandstone [Rickman et al., 1991] with α around 0.3, and a combination of pores and cracks in upper oceanic crustal rocks [Wilkens et al., 1991]. A distinct advantage of describing geometrically complex inclusions by their aspect ratio is that theoretical relationships exist which relate porosity to seismic parameters.

We obtain the aspect ratio from the ratio of width to fiberlength of an inclusion. Following Russ [1988], the width (w), is an approximation of the minor dimension of the feature and is calculated from the fundamental measurements of area and length:

$$w = \frac{4A}{\pi L} \tag{1}$$

The fiberlength (fl), an approximation of the length of the feature along its medial axis, is expressed as:

$$fl = \frac{P}{2} - \frac{2A}{P} \tag{2}$$

The second term in (2) is a correction for the finite width. Both width and fiberlength are better descriptors for elongated and bent features than length and breadth (the maximum and minimum Feret's diameter [Russ, 1988]).

The extent to which a crenulated inclusion can be approximated by an ellipse is assessed by a derived parameter, the formfactor (ff). The formfactor can be expressed in terms of the fundamental measurements of an inclusion:

$$ff = \frac{4A\pi}{P^2} \tag{3}$$

Alternatively for true ellipses the formfactor can be related to the aspect ratio by [Rickman et al., 1991]:

$$ff \simeq \frac{2\alpha}{\alpha^2 + 1} \tag{4}$$

Examination of (3) and (4) shows that similar to the definition of the aspect ratio, the formfactor is unity for a sphere and decreases with increasing ellipticity. Importantly, a comparison of the formfactors and aspect ratios calculated from the fundamental measurements by (1), (2) and (3) with those calculated from (4) provides a qualitative measure of how well the inclusions are approximated by true ellipses. Figure 2 shows a plot of formfactor against aspect ratio where the solid curve represents the formfactors calculated from (4) and the circles are the formfactors and aspect ratios calculated for the melt inclusions in BL82 (Figure 2a) and HD87 (Figure 2b). The data plot close to the analytical curve, indicating that the shape of the melt inclusions can be reasonably well approximated by ellipses.

Results

Our results show that despite the difference in melt fractions for the two experiments (Table 1) no significant difference is observed if the melt distribution is characterized by aspect ratio. Figure 3 shows a log-log plot of aspect ratio versus area of the individual melt inclusions of the two experiments. The data form a continuous trend from the smallest inclusions (by area) having the largest aspect ratios towards the largest inclusions having the smallest aspect ratios. Histograms of the aspect ratio distribution (Figures 4a, b) show that the range of aspect ratios is similar for both runs with the maximum of the distribution below an aspect ratio of 0.1.

Figures 4c and d show histograms of the percentage area of the total melt fraction versus the aspect ratio using the same bins as in Figures 4a and b. These plots demonstrate more clearly the importance of low aspect ratio melt inclusions. In runs BL82 and HD87 almost 80% and 75%, respectively, of the melt resides in inclusions with $\alpha \leq 0.1$, i.e., most of the melt resides in thin, elongated melt inclusions. In contrast, most triple junction tubules have aspect ratios around 0.2 and contain less than 20% of the melt.

There are several sources of uncertainty in our method. First, small inclusions might not be resolved; it is unlikely however that a large number of melt films in the nanometer range exist [Vaughan et al., 1982]. Second, the smaller an individual inclusion the larger the possible error in the fundamental measurements. For both cases, the error in the total area is small, since the smallest inclusions do not contribute much to the total melt fraction. A consequence of the second point is that the smallest melt

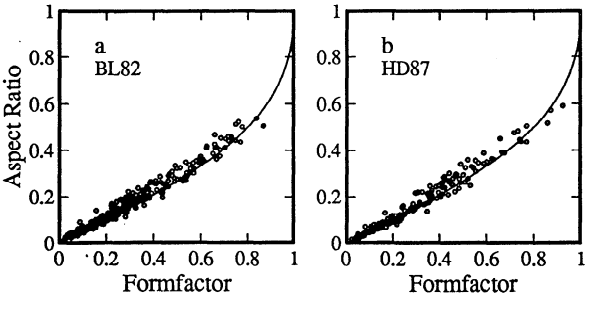

Fig. 2. Plot of formfactor versus aspect ratio. The line is the formfactor calculated from aspect ratios of true ellipses by equation (4). The circles represent the formfactor/aspect ratio pairs determined from the two experiments. (a) Data of 306 melt inclusions from BL82. (b) Data of 165 melt inclusions from HD87. The scatter at larger aspect ratios and formfactors is due to the greater uncertainties in area and perimeter of the smallest inclusions.

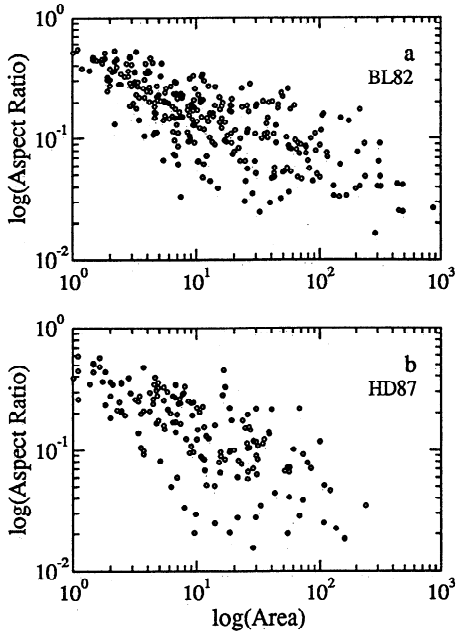

Fig. 3. Log-log plots of area versus aspect ratio of melt inclusions. (a) Data from BL82. (b) Data from HD87. The melt inclusions form a continuous trend towards decreasing aspect ratio with increasing area; the trends are similar for both samples. The largest melt inclusions, by area, have the smallest aspect ratio.

inclusions also have the largest uncertainty in aspect ratio, as these become more rounded if very thin tips are not resolved. This uncertainty results in an overestimation of the true aspect ratio. Lastly, digitization of the melt inclusions tends in most instances to overestimate the true area [Russ, 1988], so that the error in melt fraction (Table 1) is most likely smaller for the lower bound. In summary, the sources of expected uncertainty will not change our primary observation, that partial melt, by area, is mostly distributed in low aspect ratio inclusions.

Calculation of Seismic Velocities from Aspect Ratios of Melt Inclusions

Understanding the topological distribution of melt within ultramafic samples, and ultimately within the upper mantle, has several important applications, including the effect of melt distribution on seismic parameters. To illustrate this effect we use the parameters given by Schmeling [1985] to calculate the reduction in seismic velocities due to the combined effects of melt fraction and geometry. We adopt Schmeling's relationships since they extend those of O'Connell and Budiansky [1977] and Mavko [1980] to higher porosities and larger aspect ratios.

An assumption in our procedure is that the crack aspect ratios measured in two dimensions can be translated into penny-shaped cracks (oblate spheroids having two approximately equal axes much larger than the third) in three dimensions with similar aspect ratio. To test this hypothesis, numerical experiments were performed, where, instead of intersecting a random distribution of ellipsoids, the equivalent problem of intersecting a single ellipsoid with randomly oriented planes was solved. Figure 5 shows a comparison of the aspect ratio distribution resulting from the intersection of 1000 randomly oriented planes with a prolate (cigar shaped) spheroid with a ratio of length of the axes as 1:0.05:0.05 (Figures 5a, c) and an oblate spheroid (penny-shaped) with axes ratio 1:1:0.05 (Figures 5b, d). The aspect ratio distribution for the cigar-shaped ellipsoid (an approximation for the general shape of triple junction tubules) as percent fraction of all intersections has a broad range of α from 0 to 1 (Figure 5a) whereas the distribution for the penny-shaped ellipsoid has a sharp peak at $\alpha = 0.05$ (Figure 5b), recovering the original aspect ratio of the spheroid. The similarity of the aspect ratio distribution by area of the penny-shaped ellipsoids (Figure 5d) with the experimentally determined aspect ratio distribution (Figures 4c, d), suggests as a first approximation to assume the melt is contained in oblate spheroids with $\alpha = 0.05$.

While the melt distribution is clearly more complex than a representation by penny-shaped melt inclusions of one aspect ratio, this parameterization allows a significantly improved assessment of the reduction of seismic velocities due to partial melts as compared to the triple junction tubules model. The velocity reductions, per percent melt for $\alpha = 0.05$ are (unrelaxed moduli): 1.8% for V_p and 3.3% for V_s. In contrast, for melt in triple junction tubules the velocity reductions are 1% for V_p and 2.3% for V_s per percent melt. The significance of the magnitude of the velocity reductions by partial melt becomes clear when tomographic images of the upper mantle beneath volcanically active regions are interpreted in terms of the physical state. For example, large P-wave velocity contrasts (up to 8%) in the upper mantle beneath the western United States [Humphreys and Dueker, 1993] and beneath northeastern Japan [Zhao et al., 1992] in conjunction with recent volcanic activity suggests the presence of some partial melt at depth. In both cases, melt in triple junction tubules would require approximately twice as much melt to satisfy the observed velocity reductions than melt in penny-shaped inclusions.

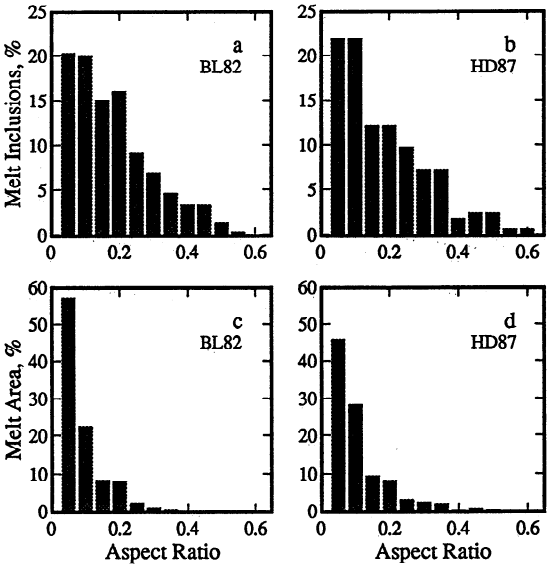

Fig. 4. Distribution of the melt by aspect ratio and by area. (a) and (c) data from BL82, (b) and (d) data from HD87. (a) and (b) show the fraction of the total number of melt inclusions having a certain aspect ratio. (c) and (d) show the area fraction for the aspect ratio distribution with the same bins as in (a) and (b). This distribution of the melt by area demonstrates most clearly the importance of the low aspect ratio melt inclusions, as they contain most of the melt. In run BL82, with a melt fraction of 3.2%, almost 80% of the melt is contained in inclusions with $\alpha \leq 0.1$. For HD87 with a melt fraction of 0.75%, almost 75% of the melt resides in inclusions with $\alpha \leq 0.1$.

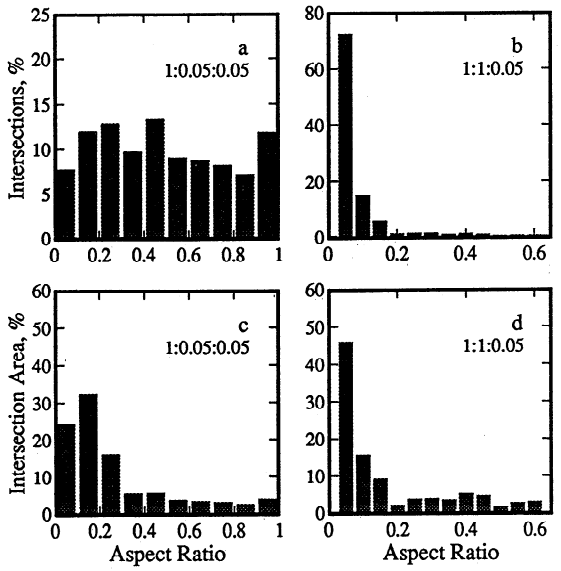

Fig. 5. Histogram showing the aspect ratio distribution of ellipses created by intersecting a prolate spheroid (a, c) and an oblate spheroid (b, d) with 1000 randomly oriented planes. (a) and (b) show the aspect ratio distribution as fraction of the total number of intersections, (c) and (d) compare the distribution by area. Note the similarity of the aspect ratio distribution resulting from the modeling of a penny-shaped ellipsoid with axes 1:1:0.05 (d) and the experimentally determined melt distribution by area (Figures 4c, d).

Summary

This paper quantifies the observations of Waff and Faul [1992] that most of the melt in ultramafic partial melts resides in melt inclusions with geometries different from those predicted by the isotropic equilibrium model. Imaging of large areas of experimentally produced samples indicates that in the two experiments examined approximately 75% of the melt occurs in inclusions with $\alpha \leq 0.1$. Low aspect ratio inclusions reduce seismic velocities much more efficiently than melt in triple junction tubules. It has also been shown that oblate spheroids with an aspect ratio of 0.05 can be used as a first order approximation of the three dimensional geometry of the imaged melt inclusions for the calculation of seismic velocities. Further work is required to determine the effects of additional solid phases and melt fraction on the melt distribution. Another effect of this melt distribution can be inferred for the permeability of partially molten aggregates: while triple junction tubules provide an interconnected network of melt, if the ellipsoidal melt inclusions do not overlap, the overall permeability will be lower than that expected for the same melt fraction residing only in triple junction tubules.

Acknowledgments. This project was supported by the National Science Foundation under grants OCE-9018389-01 and EAR-9219193. The images were collected on the CAMECA SX-50/PDP EPMA in the Department of Geological Science at the University of Oregon, funded by grants from the W.M. Keck Foundation and the National Science Foundation. We would like to thank Kathy Cashman for assistance with the image processing.

References

Bulau, J. R., H. S. Waff and J. A. Tyburczy, Mechanical and thermodynamic constraints on fluid distribution in partial melts, *J. Geophys. Res., 84*, 6102-6108, 1979.

Hadley, K., Comparison of calculated and observed crack densities and seismic velocities in Westerly granite, *J. Geophys. Res., 81*, 3484-3494, 1976.

Humphreys, E. D. and K. G. Dueker, Physical State of the western U. S. upper mantle, *J. Geophys. Res.*, in press, 1993.

Mavko, G. M., Velocity and attenuation in partially molten rocks, *J. Geophys. Res., 85*, 5173-5189, 1980.

O'Connell, R. J. and B. Budiansky, Viscoelastic properties of fluid-saturated cracked solids, *J. Geophys. Res., 82*, 5719-5735, 1977.

Rickman, D. L., F. D. Morgan and R. M. O'Leary, The shapes of pores in Berea sandstone, *Eos Trans. AGU, 72*, 490, 1991.

Russ, J. C., *Computer Assisted Microscopy, the Measurement and Analysis of Images*, North Carolina State University, Raleigh, N. C., 1988.

Schmeling, H., Numerical models on the influence of partial melt on elastic, anelastic and electrical properties of rocks. Part I: elasticity and anelasticity, *Phys. Earth Planet. Inter., 41*, 34-57, 1985.

Vaughan, P. J., D. L. Kohlstedt and H. S. Waff, Distribution of the glass phase in hot-pressed, olivine-basalt aggregates: an electron microscopy study, *Contrib. Mineral. Petrol., 81*, 253-261, 1982.

von Bargen, N. and H. S. Waff, Permeabilities, interfacial areas and curvature of partially molten systems: Results of numerical computations of equilibrium microstructures, *J. Geophys. Res., 91*, 9261-9276, 1986.

Waff, H. S. and J. R. Bulau, Experimental studies of near-equilibrium textures in partially molten silicates at high pressure, in High Pressure Research in Geophysics, *Adv. Earth and Planet. Sci., 12*, 229-236, 1982.

Waff, H. S. and U. H. Faul, Effects of crystalline anisotropy on fluid distribution in ultramafic partial melts, *J. Geophys. Res., 97*, 9003-9014, 1992.

Wilkens, R. H., G. J. Fryer and J. L. Karsten, Evolution of porosity and seismic structure of upper oceanic crust: Importance of aspect ratios, *J. Geophys. Res., 96*, 17981-17995, 1991.

Zhao, D., A. Hasegawa and S. Horiuchi, Tomographic imaging of P and S wave velocity structure beneath northeastern Japan, *J. Geophys. Res., 97*, 19909-19928, 1992.

U. Faul, D. Toomey and H. Waff,
Department of Geological Sciences, University of Oregon, Eugene, OR 97403.

(Received: July 7, 1993;
revised: October 19, 1993;
accepted: October 26, 1993.)